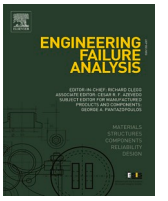
Engineering Failure Analysis 142 (2022) 106783



Contents lists available at ScienceDirect

Engineering Failure Analysis

journal homepage: www.elsevier.com/locate/engfailanal





Effect of welding processes on high cycle fatigue behavior for naval grade HSLA joints: A fatigue strength prediction

P. Hariprasath *, P. Sivaraj, V. Balasubramanian, Srinivas Pilli, K. Sridhar

Centre for Materials Joining and Research (CEMAJOR), Department of Manufacturing Engineering, Annamalai University, Annamalai Nagar 608 002, India
Naval Materials Research Laboratory (NMRL), Ambernath, Mumbai 421506, India

ARTICLE INFO

Keywords:
High strength low alloy steel
Fusion welding
S-N Curve
Tensile strength
Microhardness

ABSTRACT

Naval grade high strength low alloy steel is designed especially for shipbuilding applications due to its high strength-to-weight ratio. The fatigue failure of welded structures is susceptible to cyclic loading through heterogeneities of consumables, microstructure deformation, and complicated local stress-strain conditions. In this investigation, the influence of welding processes on high cycle fatigue behavior and fatigue strength prediction of DMR249 A grade steel. The fatigue test was conducted for five different stress levels from 50 to 90 % yield strength with a stress ratio R = −1. The evaluated fatigue properties are correlated with mechanical properties and micro-structural characteristics. The maximum obtained fatigue strength of SMAW and GMAW joints is about 342 MPa and 355 MPa for the unnotched specimens. From the experimental results, it is found that the fatigue strength of the fusion welded joints relative to 55 % (SMAW) and 59 % (GMAW) of tensile strength of the parent metal. Therefore, the fatigue strength of GMAW joints is appreciably better than SMAW joints. Finally, the constructed S—N curves of base metal and welded joints were lying above the IIW standard curve.

1. Introduction

The next generation high strength low alloy (HSLA) steels were preferred to improve the service life and performance of the shipbuilding structures [1]. The conventional welding techniques of shielded metal arc welding (SMAW) and gas metal arc welding (GMAW) are employed for the joining of these structural steels [2]. While welding, the non-uniform heating, and cooling will produce the causes of cold crack, hard HAZ, and internal residual stresses in the weldment. Other than these static causes, the heterogeneities of consumables and microstructure deformation will produce fatigue failure under cyclic loading. This heterogeneity makes weld under intricate local stress-strain conditions [3]. Therefore, the sudden catastrophic failure is necessary to avoid and improve the fatigue performance of the welded joints. The fatigue strength of steel plates has increased with operating yield stress ranges, but the tensile residual stresses and stress concentration factors affected the fatigue strength [4]. In some cases, mechanical processing and heat treatments are performed to improve the fatigue limit of the steels. However, the fatigue life prediction on different fusion welding techniques is required to improve the safety and performance of structural grade steels [5].

Zhu et al. reported the fatigue behavior of submerged arc welded Cr—Ni—Mo—V steel joints by varying frequency ranges. While

* Corresponding author.
E-mail addresses: hariprasathp12mech@gmail.com (P. Hariprasath), cemajorsiva@gmail.com (P. Sivaraj), visvabalu@yahoo.com (V. Balasubramanian), pillis.nmrl@gov.in (S. Pilli), sridsudi@gmail.com (K. Sridhar).

https://doi.org/10.1016/j.engfailanal.2022.106783
Received 20 March 2022; Received in revised form 31 August 2022; Accepted 7 September 2022
Available online 13 September 2022
1350-6307/© 2022 Elsevier Ltd. All rights reserved.

fatigue testing, the duplex-shaped S—N curve was obtained in lower range frequency. The crack initiation and final failure of welded joint depend on the loading frequency and stress level. But there is still a shortage of detailing of fatigue properties from the S—N curves in the quantitative approach because those properties are helpful to understand the fatigue behavior of welded joints in a very cycle fatigue regime [6]. Weich et al. investigated to improve the fatigue properties of the high-strength steel joints using mechanical post-weld treatments. The fatigue strength of the weld gets doubled with the presence of compressive residuals and strain hardening on the surface [7]. Wang et al. studied fatigue crack growth behavior of new generation high-strength steel. They found that the weld metal possesses better crack growth resistance relative to the parent metal under each stress ratio. But the crack is accelerated by carbides in the temper regime microstructure. The post-weld heat treatment could not eliminate the internal residual stresses in the weld, and it generated a new distribution model of residual stresses [8]. Su et al. analyzed the fatigue life predictions of laser-welded lap shear dissimilar joints by low carbon steel and high strength alloy steel. The fatigue characteristics of these weld joints have been detailed by quasi-static, low cycle, and high cycle fatigue. They estimated the fatigue life of the dissimilar joints through a local stress approach. However, there are shortcomings in the correlation between quantitative and finite element analysis results for the dissimilar welds [9]. Stoschka et al. reported that fatigue life of gas metal arc welded joints by high-strength filler metals. Whereas small and distinct changes were observed in the fatigue test of high-strength filler metal. However, the metal core wire recorded higher fatigue strength than solid wire, and the notch effect influences the fatigue characteristics in the nominal stress approach. Also, these fatigue curves have been compared with the IIW FAT curves [10]. Shiga et al. studied fatigue improvement on high-strength steel using the elongation bead weld method. They found that the overlay low-temperature transformation (LTT) method increased the fatigue properties of fusion-welded joints [11]. Ravi et al. reported the fatigue life prediction on post-weld treated strength mismatched HSLA steel joints. They found a significant improvement in fatigue life in strength mismatched weld joints. The post-weld heat treatment does not influence strength and toughness properties, but a change in residual stress magnitude was observed [12]. Moravec et al. investigated the fatigue life assessment of partial welded S700MC steel joints. These joints are severely affected by heat-affected regions during temperature cycles. Therefore, the weld joint mechanical properties and fatigue life got deteriorated [13].

From the above literature, it is understood that significant studies have fetched about structural steel. But the fatigue behavior evaluations are still deficient with quantitative results from the fatigue experiments. Although, the limited published research outcomes on fatigue life prediction of fusion welded naval grade steel joints. Hence, this investigation aims to analyze the influence of welding processes on mechanical properties, microstructural characteristics, and fatigue behavior of DMR 249A grade steel for shipbuilding structures.

2. Scheme of experimentations

2.1. Materials specification and properties

The rolled naval grade HSLA steel had procured with a thickness of 13 mm for this investigation. The chemical composition and mechanical properties of base metal and filler metals had provided in Tables 1 and 2. The microalloying elements have assisted the superior material properties and ferrite-pearlite microstructures formation. Fig. 1 shows the base metal microstructure of naval grade steel, which comprises 95 % ferrite and 5 % pearlite.

2.2. Welding experimentation and fatigue testing

For joining, the HSLA steel plates are prepared as a single V notch (60°) with a dimension of 150 × 150 × 13 mm. Before welding, the cleaning of mating surfaces to avoid cold cracking or foreign particle inclusion in the weldment. The welding experiment had carried out through typical manual metal arc welding and gas metal arc welding processes (Make: Lincoln Electric; model: precision 375) (Make: Lincoln Electric; model: Power wave 455 M/STT). The consumables used for this investigation are E8018 – G and ER80s. Table 3 exhibit the welding parameters of SMAW and GMAW joints. Fig. 2 a-b represented the joint configuration and fabricated SMAW and GMAW joints. The fabricated weld joints were analyzed with X-ray radiography to qualify the defect-free weld joints. Then, the specimen extraction and mechanical tests have performed as per the ASTM E08-13 standard (Fig. 2c-d). The transverse tensile test was to be executed through a semi-automatic servomotor-controlled UTM machine with a capacity of 1000 kN (make: FIE Bluestar; model: 100HGFL). The impact toughness test had accomplished using a manually controlled impact testing machine with a capacity of 300 J (Make: FIE Bluestar; Model: 1E-IT-30). And, Microhardness measurements were carried out using Vicker's microhardness testing machine with tentative conditions of 500 g load and 15 *sec* dwelled time (Make: Shimadzu; Model: HMV 2 T). Afterward, the welded coupons were cross-sectioned to evaluate the weld quality and characteristics using stereo zoom macroscopy and optical microscopy (Make: Huvitz; Model: HRM 300). The cross-sectioned metal coupon was mounted and polished using ultrafine grain diamond paste. Besides, the polished specimen was etched with freshly prepared Nital with an etching time of 30–60 *sec*.

Table 1
Chemical composition (wt %) of Base metal and Filler metal.

Elements	C	Mn	Cr	N	Si	Mo	Ti	V	Nb	Ni	Cu	Al	Fe	CE
DMR 249A	0.099	1.45	0.03	0.02	0.21	0.001	0.03	0.04	0.04	0.71	0.18	0.03	bal	0.44
E8018-G	0.08	1.4	0.01	0.009	0.2	0.15	0.02	0.01	0.02	2.3	0.05	0.015	bal	0.41
ER80S	0.08	1.3	0.02	0.008	0.3	0.17	0.01	0.02	0.023	2.8	0.035	0.014	bal	0.45

Table 2
Mechanical properties of Base metal and Filler metal.

S.No	0.2 %Yield strength (MPa)	Ultimate Tensile strength (MPa)	Elongation in 50 mm gauge length (%)	Notch Tensile strength (MPa)	Notch strength Ratio (NSR)	Impact strength at RT (J)	Vickers hardness at 0.5 kg load (Hv)
DMR 249A	485	614	28	654	1.05	208	273
E8018-G	521	625	22	–	–	190	290
ER80S	515	620	21	–	–	195	293

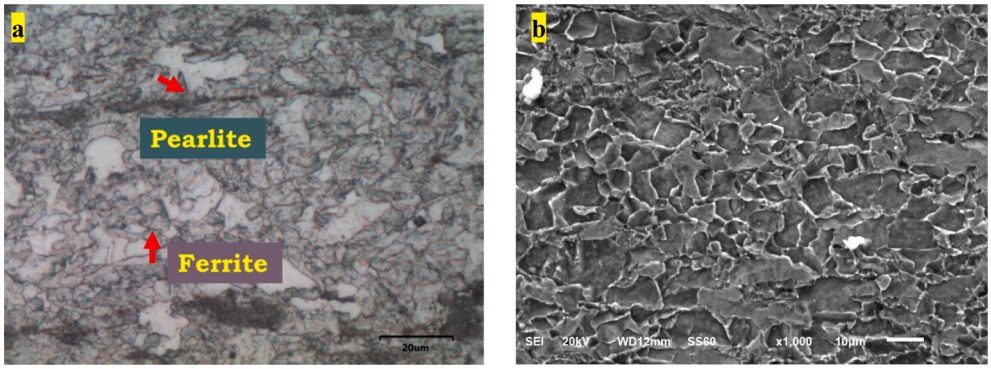


Fig. 1. (a-b) Optical and scanning electron microstructure of DMR249A grade steel.

Table 3
Welding parameters and conditions used to fabricate the joints.

Welding Parameters	SMAW		GMAW	
	Root Pass	Capping Pass	Root Pass	Capping Pass
Filler metal	E 8018G-C1	E 8018G-C1	ER80s	ER80s
Filler diameter/mm	3.2	4	1.2	1.2
Pre-heating Temperature °C	100	100	100	100
Inter pass Temperature °C	125	125	125	125
Current/A	110	165	155	195
Voltage/V	21	27.5	22	29
Welding speed/(mm/min)	145	153	160	170
Heat input/(kJ/mm)	1.066		1.278	
Cumulative Heat Input (kJ)	6.6		6.01	
No. of Passes (Include Capping)	6		5	

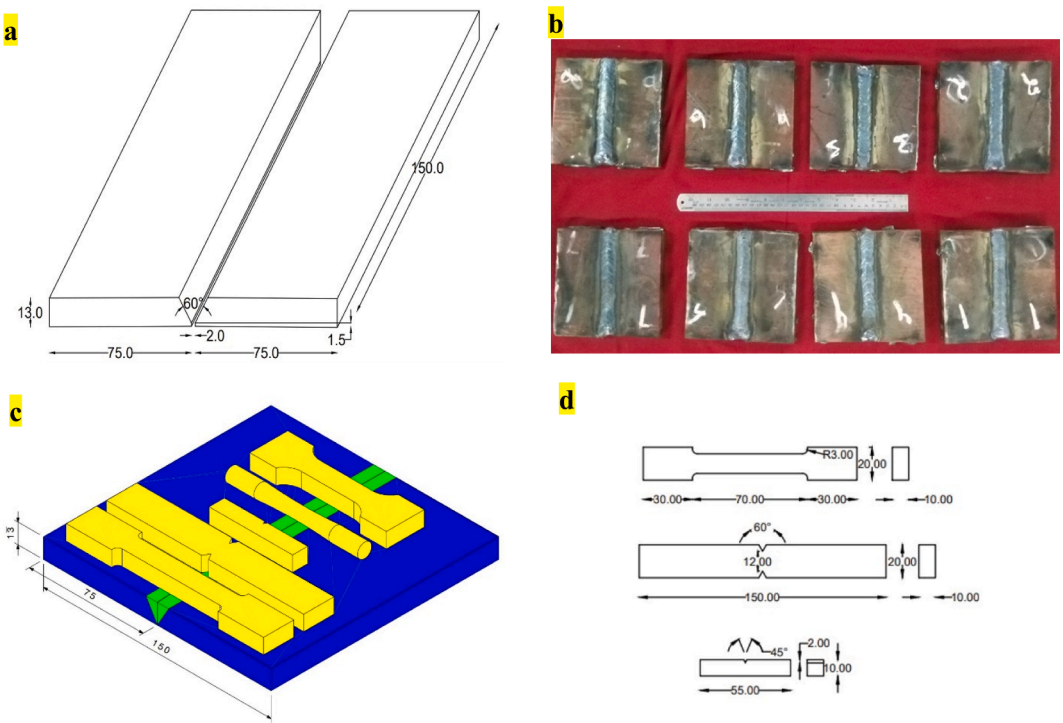


Fig. 2. (a) Joint configuration; (b). Fabricated SMAW & GMAW joints; (c). Specimen extraction diagram; (d). Dimension of notched, unnotched tensile & Impact specimens.

After mechanical properties evaluation, the fatigue testing has undergone fully reversed cycle fatigue testing using the Instron fatigue machine (Make: Instron; Model: R.R. Moore). The fatigue test had conducted for both parent metal and welded joints with a stress range of 50–90 % yield strength. The sine type of cyclic loading had applied with a stress ratio R = −1. The test shutdown criteria of 10^7 cycles fixed for the high cycle fatigue. A cylindrical straight shank smooth and center notch specimen was used for rotary beam fatigue testing, and the photograph and specimen dimensions showed in Fig. 3 (a-b). The fabricated coupons prepared under ASTM 466 standard, which has reduced section constrains the failure at mid-section. Before fatigue testing, all the fatigue specimens were polished and maintained with a roughness of 0.1 μm. After that, the surface topographic was analyzed using scanning electron microscopy (SEM) and detailed the features of the failure (Make: Jeol: Model: JSM 7900F).

3. Results

3.1. Tensile and impact toughness properties

The transverse tensile test had used to measure the load-bearing capacity of the fabricated joints. The tensile test of fusion-welded joints was conducted, as per the ASTM E-08-13a standard. The maximum obtained yield strength and ultimate tensile strength of welded joints were 473 & 558 MPa (SMAW) and 480 & 570 MPa (GMAW). While tensile testing, most of the weld failures occurred subcritical interface region. And the ductile mode of failure was observed from both welded joints, which confirmed with notch strength ratio (NSR) higher than the unity value [14]. Though, the impact test performed for SMAW and GMAW joints and its toughness values achieved about 174 & 178 J. The impact samples observed better impact toughness properties due to the alloying elements [15]. Table 4 presented the mechanical properties of the corresponding fusion-welded joints. The prescribed table values are mean strength values by the average of three test results.

3.2. Microhardness measurement

The microhardness study had performed across the fusion-welded joints. Fig. 4 shows the hardness distribution for the various zones (FZ, CGHAZ, FGHAZ, and BM) of SMAW and GMAW joints. The hardness differences mainly occurred based on the heat dissipation from the weld center. The weld region recorded a moderate improvement in hardness compared to the base metal and the corresponding value of 310 HV and 285 HV for GMAW and SMAW, respectively. Next, the coarse grain HAZ recorded a maximum hardness of 475 HV at GMAW and 463 HV at SMAW. Also, this higher microhardness confirms the segregation of major alloying elements from the fusion interface [16]. Subsequently, the hardness drop had recorded in the fine grain HAZ region (248 HV). The lowest hardness was obtained in the subcritical HAZ region at 175 HV. These hardness profiles have more relative agreement with strength levels in the welded joints [17].

3.3. Macrostructure and microstructure

The macrostructure examination has distinguished the visual defects and various zones in the weld cross-section. Here, the high-strength naval grade steel plates had welded with full penetration and defect-free sound weld joints [18]. Fig. 5 (a-b) presents the macrostructure of SMAW and GMAW joints. The identified different zones such as fusion zone (FZ), coarse grain heat-affected zone (CGHAZ), fine grain heat-affected zone (FGHAZ), and base metal (BM).

From the microstructural analysis, the fusion zone has a fine grain at the bottom layer and long columnar grains at the capping section (Fig. 6 a&e). The bottom and top layer microstructures are relative to SMAW and GMAW joints. The fusion region contains Widmanstädten ferrite, acicular ferrite, bainite, and pearlite microstructure [19]. These morphologies confirm with high magnification TEM microstructure; it shows upper bainite structure in the welded joints (Fig. 7 a-b). Next to the fusion region, the coarse grain HAZ formed due to plastic strain and severe heat dissipation rate from the weld center [20]. The CGHAZ contains bainite and acicular ferrite

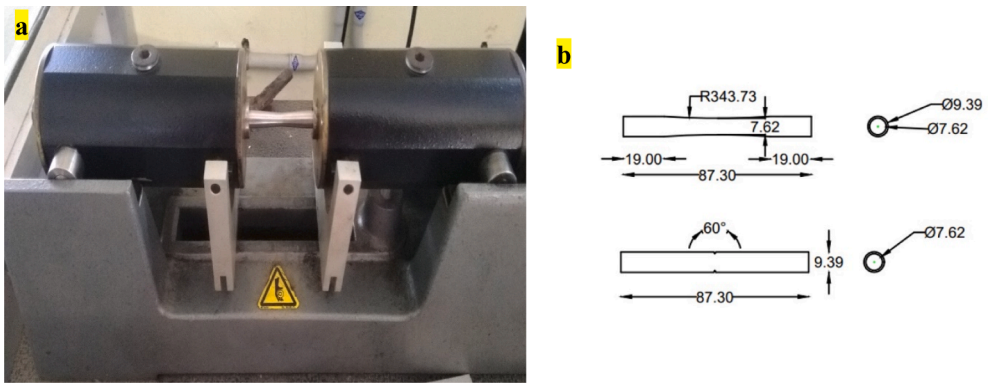


Fig. 3. (a) Photograph of fatigue machine; (b). Schematic diagram for fatigue specimen.

Table 4
Tensile and Impact properties of SMAW and GMAW joints.

Joints	Yield strength (MPa)	Ultimate Tensile strength (MPa)	Elongation (%)	Notch Tensile strength (MPa)	Notch strength Ratio (NSR)	Impact strength at RT (J)	Vickers hardness at WM 0.5 kg load (Hv)	Joint Efficiency (%)	Failure location
SMAW	473	558	19	578	1.03	174	304	88	**HAZ - BM interface**
GMAW	480	570	17	585	1.04	178	307	92	**HAZ - BM interface**

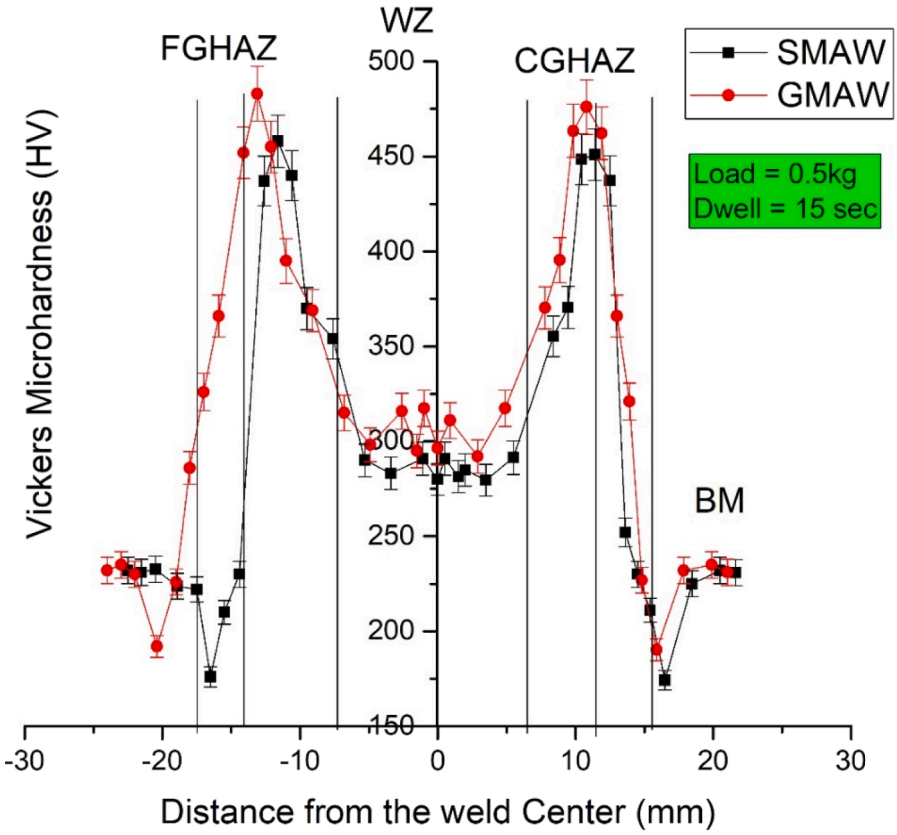


Fig. 4. Microhardness measurement across the mid thickness.

microstructure in the deformed section, as per Fig. 6 b &f. Similarly, Fig. 6 c & g revealed fine-grain HAZ; it is comprised of fine-ferrite grains. In FGHAZ, the impact of elastic distortion is minimal, so the hardness value nominally higher than the base metal [21]. Further, the subcritical interface zone shows the combination of polygonal ferrite and pearlite microstructure in temper conditions (Fig. 6 d& h). Therefore, the destructive hardness test recorded lower hardness in these regions. And, the weld failure accelerated in the subcritical interface region.

3.4. Fatigue behavior of base metal and welded joints

3.4.1. S—N curve

The S—N curve has developed a relationship between applied cyclic stress and fracture number of cycles to the material. The fatigue test had performed through five levels of yield strength and a fully-reversed stress cycle (R = −1). The termination criteria for the fatigue samples to achieve the 10^7 cycles as fatigue limit . The S—N curves presented notch and unnotched specimen results of base metal, SMAW, and GMAW joints as per Fig. 8. Interestingly, the observed S—N curves have the same tendencies in negative stress ratio criteria in both base metal and welded joints. Also, the dispersion band (95 % confidence interval) was constructed along with the mean regression fatigue curve. Here, the decrease of applied stress clearly states that increasing the number of cycles to failure of the specimens. From the S—N curve, the Basquin fatigue relationship has developed.

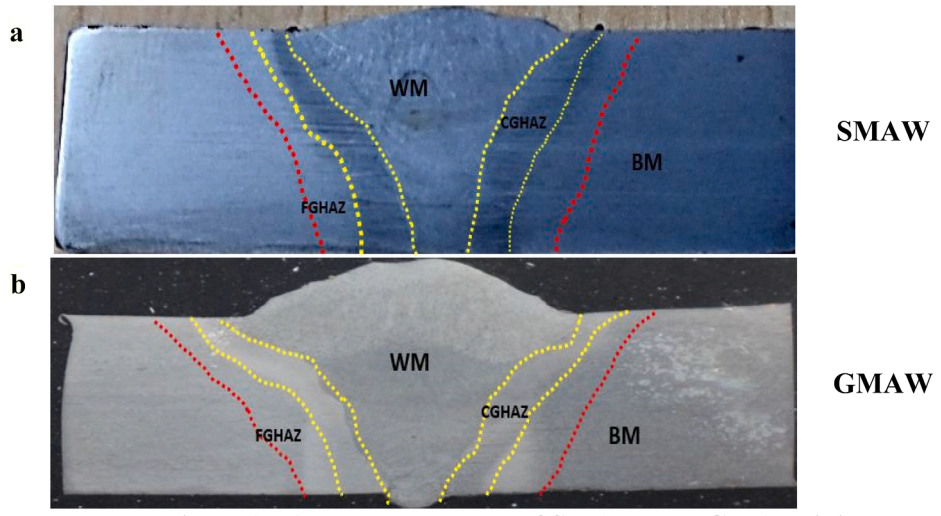


Fig. 5. (a-b) Macrostructure of SMAW and GMAW joints.

$$\boldsymbol{C} = (\boldsymbol{\sigma_a})^{p}\boldsymbol{N}$$

$$\boldsymbol{N_f} = \boldsymbol{C}(\boldsymbol{\sigma_a})^{2.7}(\boldsymbol{Base})$$

$$\boldsymbol{N_f} = \boldsymbol{C}(\boldsymbol{\sigma_a})^{3.5}(\boldsymbol{SMAW})$$

$$\boldsymbol{N_f} = \boldsymbol{C}(\boldsymbol{\sigma_a})^{3.8}(\boldsymbol{GMAW})$$

The Basquin model derived the fatigue life equation for base metal, SMAW, and GMAW joints. The slope (p) and intersection (C) values were yielded through the S—N curve. This equation corresponds to the number of cycles to failure (N_f) and alternate stress (σ_a). Though, the fatigue strength of the material has been decided as 2×10^6 cycles as IIW recommended standard [22]. Table.5 presents the evaluated fatigue properties of base metal and welded joints. Among the tested samples, the fatigue strength of base metal, SMAW, and GMAW joints were 394 MPa, 342 MPa, and 355 MPa, respectively.

While fusion welding, the internal residual stress is interlocked within the joints, and these residuals drop the fatigue properties of the weld joints. According to Muhayat et al., fatigue strength is the strength of the weakest atomic bonding of the material; if the fatigue strength of the material decreases confirms the presence of fissure defects [23]. Here, the fatigue fracture occurred at the center of the sank specimen. Subsequently, the fatigue testing of the notched specimen was carried out on base metal and welded joints to understand the notch effect. The notch sensitivity increases the stress intensity factor, which accelerates fatigue failure of the material [24]. The recorded notch fatigue strength for the base metal (340 MPa), SMAW (304 MPa), and GMAW (314 MPa) samples. Among the welded samples, the GMAW joints have a moderate improvement in fatigue strength then SMAW joints [25]. However, the fatigue notch factor (K_f) and notch sensitivity factor (q) has observed from the S—N curve. The fatigue notch factor increases the tendency to fatigue crack resistance was lower [26,27]. Similarly, a notch sensitivity factor decreases with improved crack resistance during cyclic stress. Then, the fatigue results of naval grade steel compared with IIW recommended FAT classes [28,29]. The FAT 80 curve was suggested by IIW FAT class for the butt joint with a slope of $m = 3$. For this IIW criterion, the base metal and weld joints recorded higher fatigue strength than the FAT classes [30]. Although, the S—N curve of base and welded joints are lying above the standard FAT limit.

3.5. Fractography analysis

The fractography typically helps to reveal failure mode in the welded joints. The tensile specimen failure occurred in the subcritical HAZ region and it has been unveiled as a cup-cone fracture (Fig. 9 i - ii). Fig. 9 (a-b) shows the propagation of the fracture surface, which is composed of a large number of dimples features. This fibrous morphology is a measuring index for its ductile nature [31]. Similarly, the tensile notch specimen has dimples and microvoids, as shown in Fig. 9 (c-d). The size of dimples can directly influence on properties of the weldments. Then, the scanned image of impact-tested samples and corresponding fractography for SMAW and GMAW joints as presented in Fig. 10 (a-d). The impact sample exhibited wave marks and dimples features. The dimple feature is evident for better toughness property in both welded joints [32].

Further, Figs. 11–13 revealed the scanned image of the fractured fatigue specimen and the corresponding failure pattern of base metal and welded joints. The fatigue life of the material depends on the ratio of crack initiation time and crack propagation time on a fractured surface [33]. Fig. 11a shows the scanned failure image of base metal, which consist of initiation, propagation, and

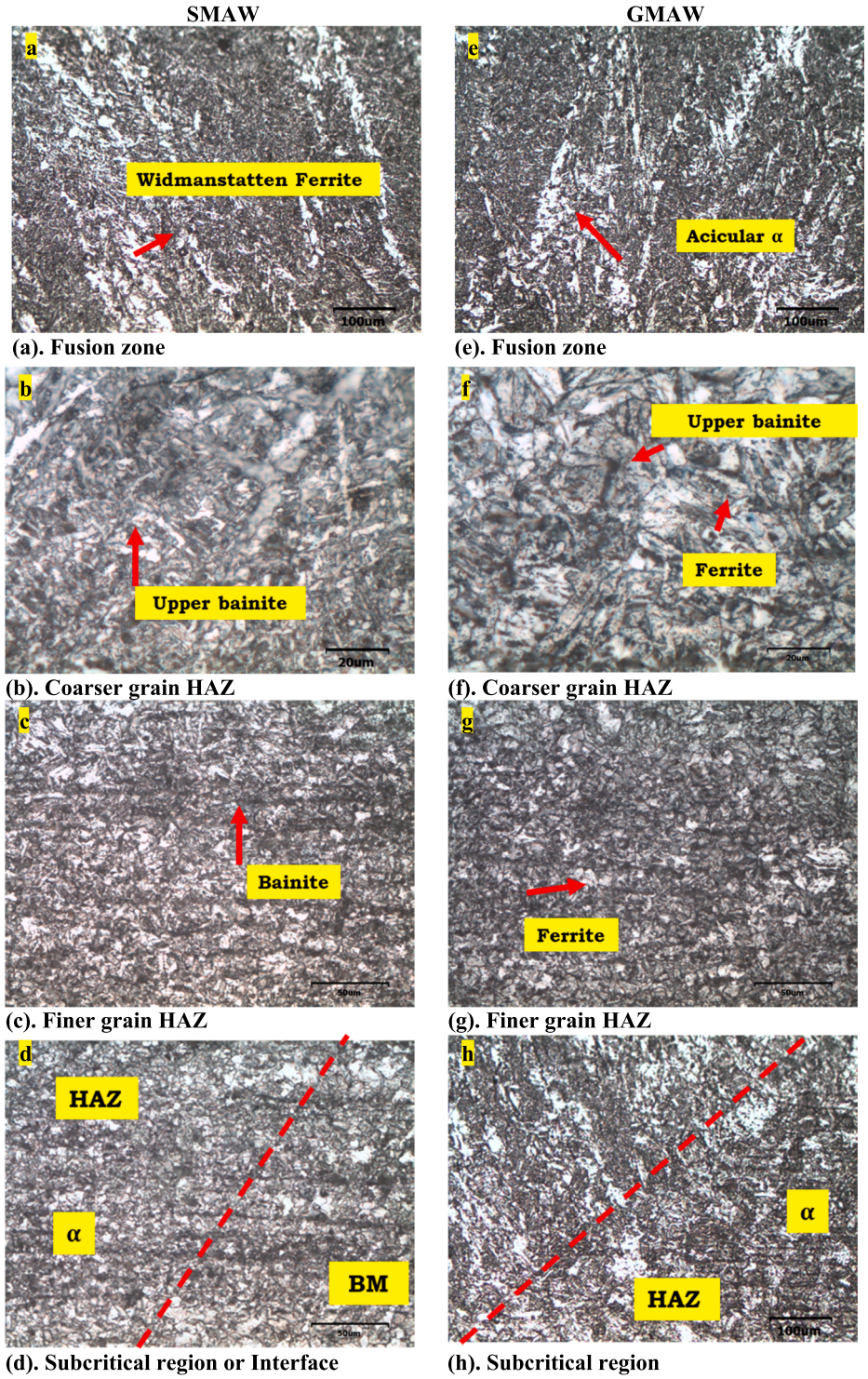


Fig. 6. Microstructure of SMAW and GMAW joints (a&e). Fusion zone; (b&f). Coarser grain HAZ; (c&g). Finer grain HAZ; (d&h). Subcritical region or Interface.

disintegration section. Similarly, Fig. 12a & 13a illustrated scanned fractured images of SMAW and GMAW joints. In HCF, the crack initiation is accelerated by applied stress through micro-fissures on the surface. The crack initiation reveals beak marks and wave patterns, as shown in Fig. 11b. Hence, the fractography of welded joints also observed wave patterns and beak marks (Fig. 12b & 13b). The crack initiation is readily connected with the crack propagation region (Fig. 11c, 12c, and 13c), which consists of fine striation

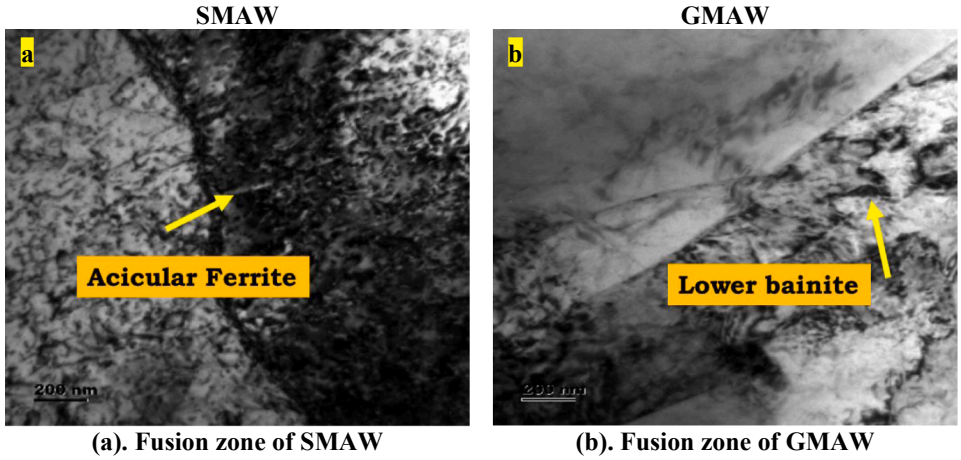


Fig. 7. (a-b) TEM Microstructure of SMAW and GMAW joints.

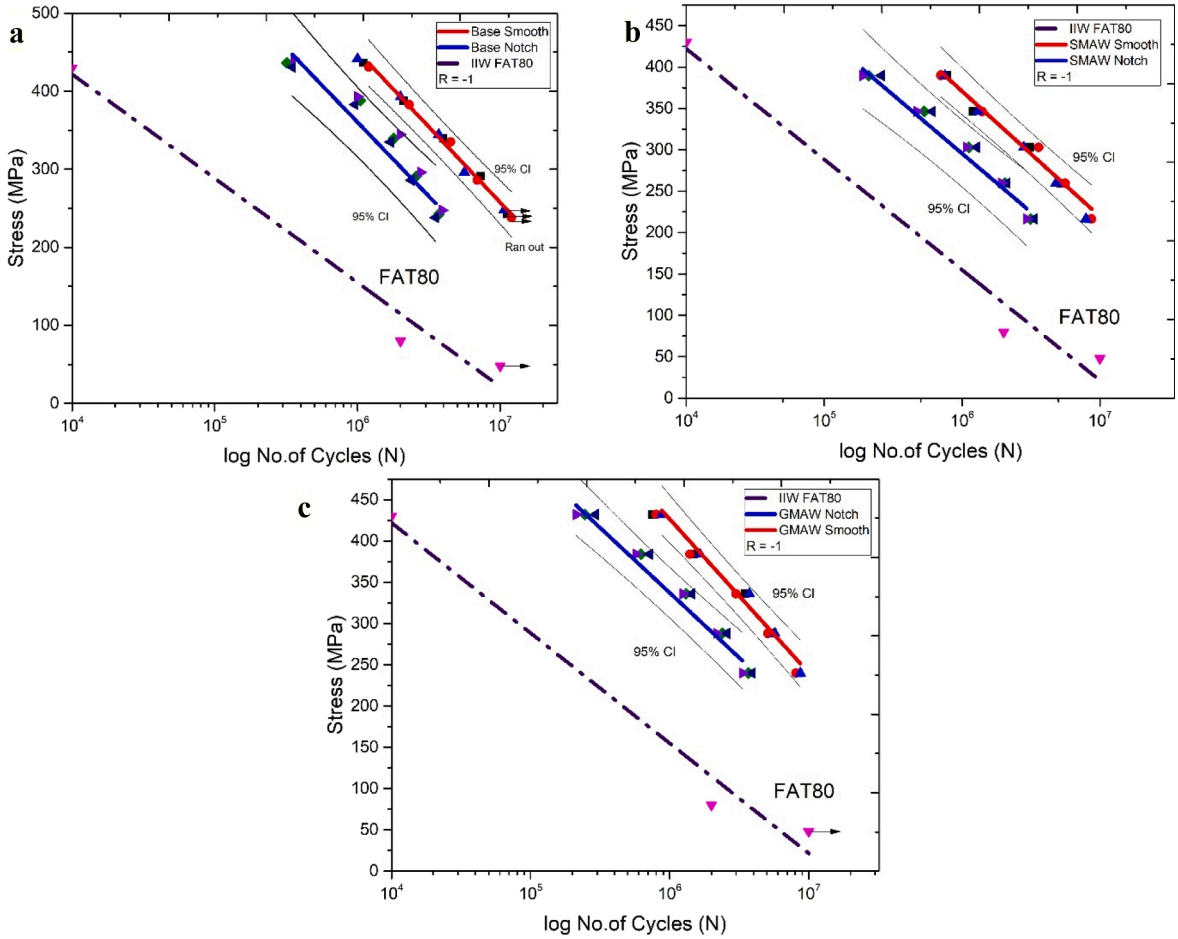


Fig. 8. S—N curve for stress ratio R = −1. (a) Base metal; (b). SMAW; (c). GMAW.

marks in the base metal and welded joints. The striation feature confirms the nature of fatigue fracture in the materials [34]. Fig. 11d, 12d, and 13d revealed the disintegration section of base metal, SMAW, and GMAW joints. This fracture section disclosed the presence of beach marks and tear rips.

Table 5
Fatigue Properties of base metal and welded joints for R = -1.

Joint type	Slope of the S—N Curve, p	Intercept of the S—N Curve, C	Fatigue strength of unnotched specimen at 2×10^6 cycles, MPa	Fatigue strength of notched specimen at 2×10^6 cycles, MPa	Fatigue Notch factor, K_f	Notch sensitivity factor, q
BM	2.7	5.1×10^{19}	394	340	1.15	0.75
SMAW	3.5	5.4×10^{24}	342	304	1.11	0.83
GMAW	3.8	4.2×10^{26}	355	314	1.13	0.8

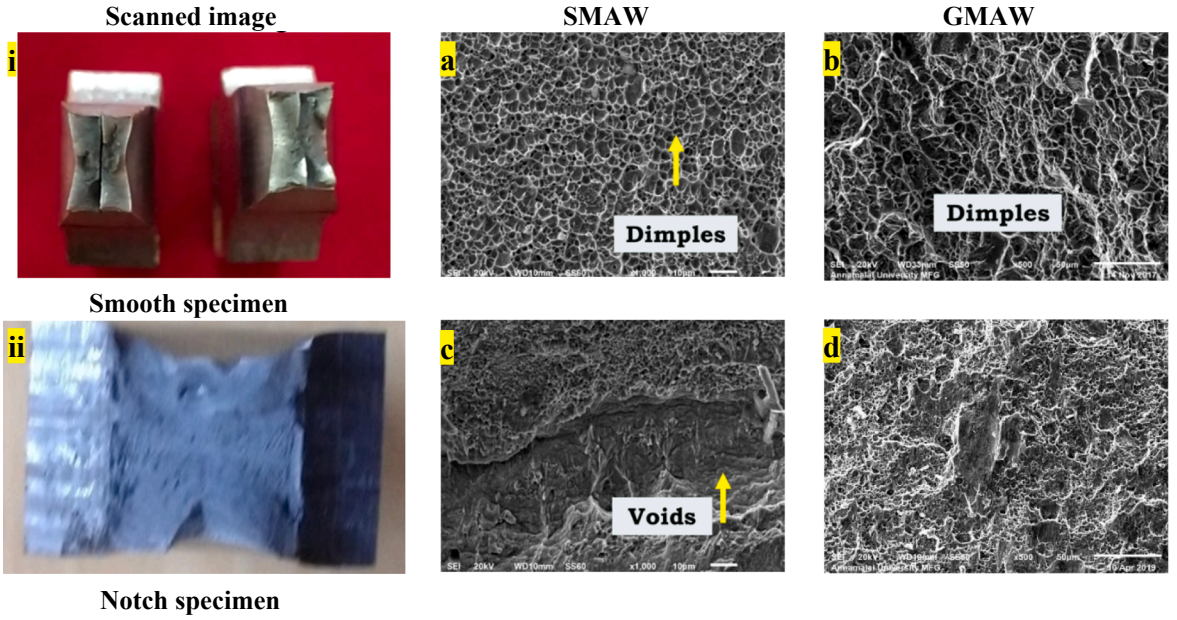


Fig. 9. SEM fractography of tensile specimens: (i - ii). Scanned image of smooth and notch specimen; (a-b). Smooth specimens of SMAW and GMAW; (c-d). Notch specimens of SMAW and GMAW.

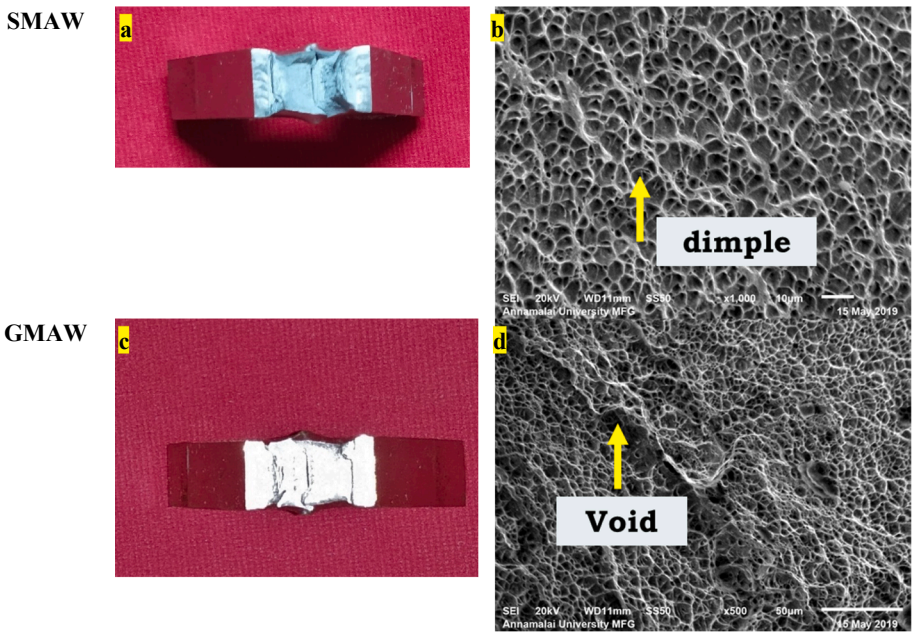


Fig. 10. Scanned image and SEM fractography of Impact specimens. (a-b) SMAW; (c-d) GMAW.

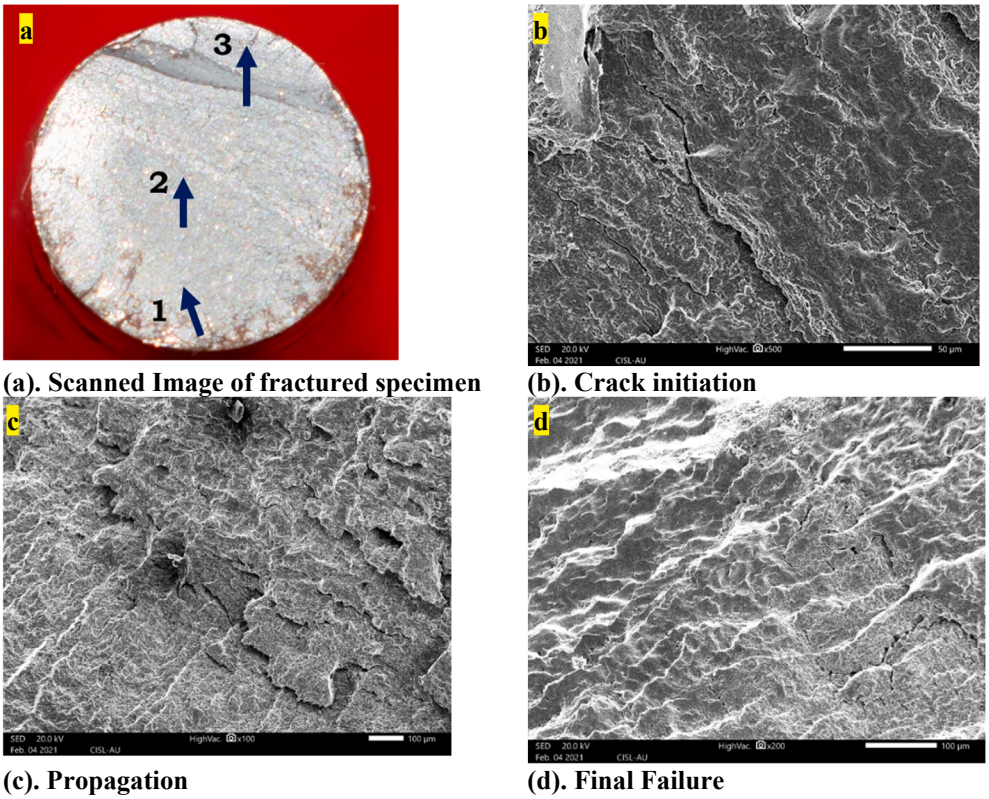


Fig. 11. SEM fractography of unwelded parent metal: (a) Scanned image; (b) Crack initiation; (c). Propagation; (d). Final Failure.

4. Discussion

4.1. Effect of mechanical properties and microstructural characteristics on fatigue behavior

The development of new age materials is to enhance the service life and performance of the structural components. The DMR 249A is an HSLA steel specially designed for navy structure. For this steel, a welding-related study is required to improve its safety and performance. In this research, the mechanical properties revealed that the weld joints are relatively equal to the parent metal properties [35,36]. The tensile joint efficiency of SMAW and GMAW was about 88 % and 92 %. Here, the tensile failure was initiated and accelerated through the HAZ interface. This sensitive region has formed due to the tempering of grains by heat dissipation from the weld center [37]. Then, the impact test results exhibited better toughness properties in base metal and weld metal. This combination of tensile strength and toughness properties attributes to the fatigue behavior of welded joints [38]. The hardness graph revealed that the subcritical HAZ region is prone to weld failure [39]. Also, a higher hardness was reported in coarser grain HAZ. According to Walter et al., the hardness has more relationship with the fatigue strength of the material. If the hardness is higher, the material will perform excellent cracking resistance during cyclic loading [40].

The weld metal microstructure is composed of acicular ferrite, Widmanstädten ferrite, and bainite phases. The acicular ferrite (AF) microstructure is a common microstructure observed in steel weldment during a moderate cooling rate [41]. This AF morphology consists of fine grain size (1 – 4 um) and a large number of high angle grain boundaries (HGB), which attributes higher hardness and strength properties of welded joints [42]. Also, the AF microstructure needle branches help to reduce the stress intensity factor on fatigue crack initiation on the weldments [43]. The above statements of acicular ferrite microstructure agreed with studies of nugoula et al. [44]. Hence, the fabricated joint using the GMAW process exhibited higher tensile strength and fatigue strength than the SMAW. Because the volume fraction of AF microstructure was higher in the GMAW joint.

4.2. Fatigue behavior on rotary beam fatigue testing

In the rotary beam fatigue test, the cylindrical specimen experienced tensile and compression stress at the top and bottom sides. While rotating, the bottom side would open the fissure cracks by tensile stress, and the top side was closed by compressive stress [45]. These compressive and tensile loads were cyclic manner until the specimen experiencing the transition stage between the fatigue to overload condition [46]. Here, the number of cycles increases with reducing stress levels, and the fatigue strength has denoted by the weakest bond or defective region strength. Then, the notched specimen resulted in lower fatigue strength than the unnotched fatigue

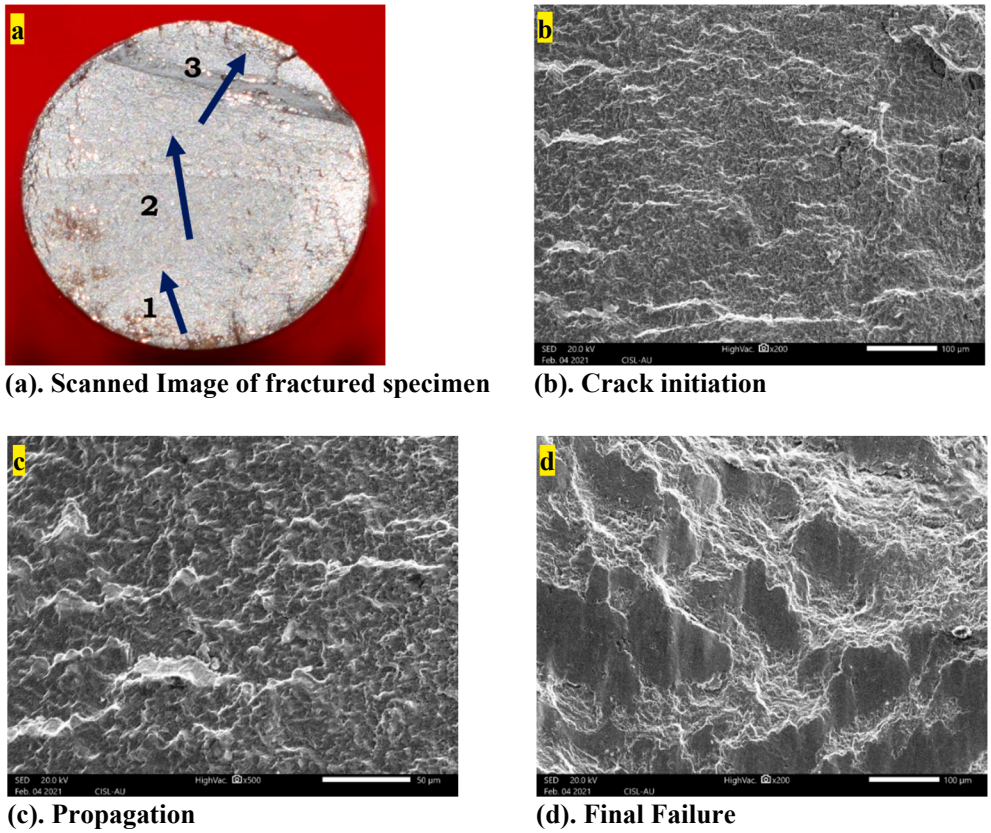


Fig. 12. SEM fractography of SMAW joints: (a) Scanned image; (b). crack initiation; (c). Propagation; (d). Final Failure.

specimen, and it is due to the notch sensitivity effect on the notched specimen [47]. The tensile residual stresses are the main factor for reducing fatigue strength in the fusion welded joints under constant cyclic loading conditions stated by Ravi et al. Also, they have studied the influence of mismatch ratio in HSLA welded joints [48]. However, the fatigue test results revealed that GMAW joints have better fatigue life than the SMAW joints. Though, the recent fatigue-related work dealing with mechanical treatments to improve the fatigue properties of welded joints by Yildirim et al. [49]. But this study has fulfilled the current requirements of shipbuilding criteria with improved parent and weld joint properties. For validation, the fatigue results of base metal and welded joints are compared with IIW FAT classes. The IIW standard recommended FAT 80 class (m = 3) as Butt joints for the naval grade steels. The comparison curves revealed that base metal and welded joints sat above the FAT80 class standard curve.

4.3. Effect of welding processes on fatigue behavior

The effect of fusion welding techniques was correlated using different heating and cooling rates of the weldment. The formation and distribution of ferrite microstructure were controlled by heat input. If the heat input is higher the acicular ferrite (AF) formation is lower, which attributes to the growth of polygonal ferrite in the weldment [50]. Also, the cooling rate plays a vital role in the grain growth of the weldment. In this research work, the recorded cumulative heat input of SMAW and GMAW was 6.6 kJ and 6.01 kJ. The accumulative heat input of GMAW is lower compared to the SMAW process [51]. Therefore, the GMAW weldment has a higher cooling rate, which attributes to that large volume of AF microstructure. This AF microstructure offers better fatigue crack resistance of the GMAW sample over SMAW. Hence, the fatigue behavior study in different welding techniques gives attention to component fabrications in ship structures.

5. Conclusion

The present research analyzes the effect of welding techniques on the rotary beam fatigue behavior of naval-grade steel. From the above study the following conclusions were made:

- In a fully reversed cycle, the fatigue performance of welded joints is lower compared to the base metal. Here, the welding residuals lead to drops in fatigue strength in the welded joints.
- The tensile strength and hardness properties are controlling factors of fatigue behavior of welded joints.

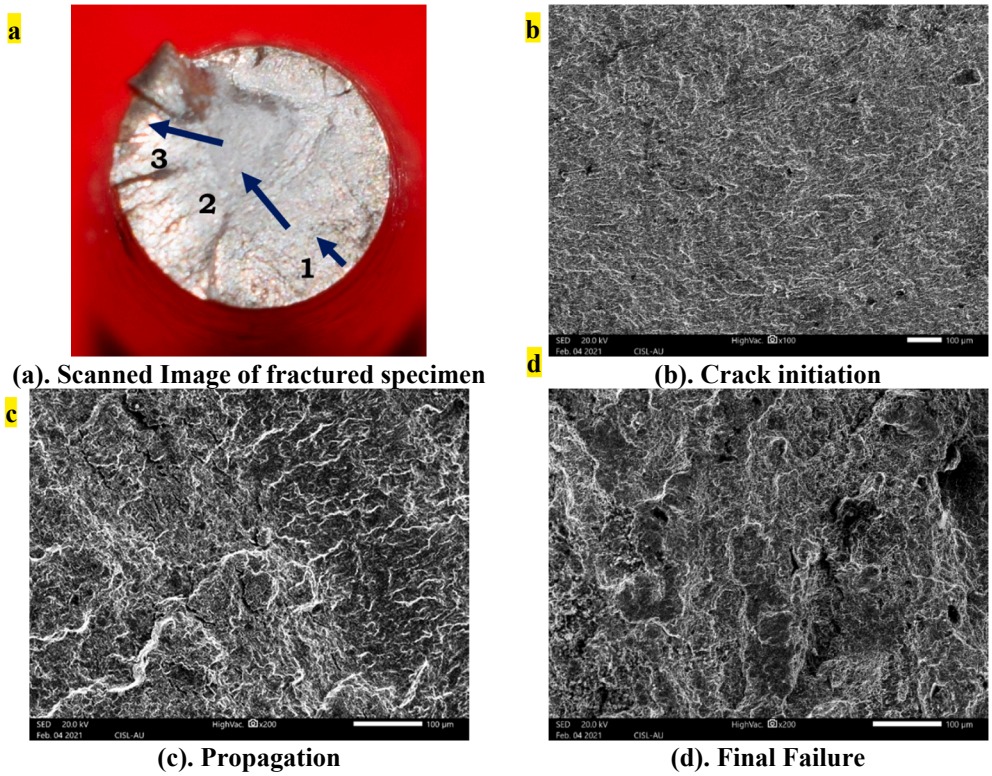


Fig. 13. SEM fractography of GMAW joints: (a) Scanned image; (b). crack initiation; (c). Propagation; (d). Final Failure.

- The fatigue resistance of the GMAW joint was higher compared to SMAW in a fully reversed stress cycle. Metallurgically, this is due to a higher volume fraction of ferrite microstructure. Also, the productivity of the GMAW process has enhanced the fatigue crack resistance over the SMAW process.
- From this investigation, it is found that the fatigue strength of the fusion welded joints relative to 55 % (SMAW) and 59 % (GMAW) of tensile strength of the parent metal. This finding is beneficial for the fabrication of shipbuilding components using SMAW and GMAW techniques.
- The fractography and surface morphologies are in addition to the fatigue failure, which shows the transition phases of fatigue modes from initiation, crack propagation, and final fracture. These finding helps deepen our understanding of the influence of welding processes on naval-grade steel.
- For validation, the constructed S—N curves have been compared with IIW FAT 80 class for butt joints. However, all the constructed S—N curves sat above IIW standard curve.

Declaration of Competing Interest

The authors declare that they have no known competing financial interests or personal relationships that could have appeared to influence the work reported in this paper.

Data availability

Data will be made available on request.

Acknowledgements

The authors express gratitude to the Director, Naval Research Board (NRB-DRDO), New Delhi, India for the financial support rendered through R & D project (Project number: NRB-443/MAT/18-19). And, the authors thanks to Naval Materials Research Laboratory (NMRL-DRDO), Mumbai, India for providing base materials to carry out this investigation.

References

[1] H.C. Yıldırım, Recent results on fatigue strength improvement of high-strength steel welded joints, Int. J. Fatigue 101 (Aug. 2017) 408–420, https://doi.org/10.1016/J.IJFATIGUE.2016.10.026.

[2] S. Tsutsumi, R. Fincato, P. Luo, M. Sano, T. Umeda, T. Kinoshita, T. Tagawa, Effects of weld geometry and HAZ property on low-cycle fatigue behavior of welded joint, Int. J. Fatigue 156 (2022) 106683.

[3] M. Mosallaee, M.T. Semiromi, Effect of nickel content on the microstructural, mechanical and corrosion behavior of E7018-G electrode weld metal, J. Mater. Eng. Perform. 30 (12) (2021) 8901–8912, https://doi.org/10.1007/s11665-021-06100-9.

[4] N. Guo, D. Liu, W. Guo, H. Li, J. Feng, Effect of Ni on microstructure and mechanical properties of underwater wet welding joint, Mater. Des. 77 (Jul. 2015) 25–31, https://doi.org/10.1016/J.MATDES.2015.04.007.

[5] R. Ghomashchi, W. Costin, R. Kurji, Evolution of weld metal microstructure in shielded metal arc welding of X70 HSLA steel with cellulosic electrodes: A case study, Mater. Charact. 107 (Sep. 2015) 317–326, https://doi.org/10.1016/J.MATCHAR.2015.07.032.

[6] M.L. Zhu, L.L. Liu, F.Z. Xuan, Effect of frequency on very high cycle fatigue behavior of a low strength Cr–Ni–Mo–V steel welded joint, Int. J. Fatigue 77 (Aug. 2015) 166–173, https://doi.org/10.1016/J.IJFATIGUE.2015.03.027.

[7] I. Weich, T. Ummenhofer, T. Nitschke-Pagel, K. Dilger, H. Eslami Chalandar, Fatigue behaviour of welded high-strength steels after high frequency mechanical post-weld treatments, Weld. World 53 (11) (2009) R322–R332, https://doi.org/10.1007/BF03263475.

[8] Q. Wang, Z. Yan, X. Liu, Z. Dong, H. Fang, Understanding of fatigue crack growth behavior in welded joint of a new generation Ni-Cr-Mo-V high strength steel, Eng. Fract. Mech. 194 (May 2018) 224–239, https://doi.org/10.1016/J.ENGFRACMECH.2018.03.016.

[9] Z.M. Su, P.C. Lin, W.J. Lai, J. Pan, G.J. Cheng, H.W. Yen, Fatigue analyses and life predictions of laser-welded lap-shear specimens made of low carbon and high strength low alloy steels, Int. J. Fatigue 140 (Nov. 2020), 105849, https://doi.org/10.1016/J.IJFATIGUE.2020.105849.

[10] M. Stoschka, M. Leitner, G. Posch, W. Eichlseder, Effect of high-strength filler metals on the fatigue behaviour of butt joints, Weld. World 57 (1) (2013) 85–96, https://doi.org/10.1007/s40194-012-0010-6.

[11] C. Shiga, H. Murakawa, K. Hiraoka, N. Osawa, H. Yajima, T. Tanino, S. Tsutsumi, T. Fukui, H. Sawato, K. Kamita, T. Matsuzaki, T. Sugimura, T. Asoda, K. Hirota, Elongated bead weld method for improvement of fatigue properties in welded joints of ship hull structures using low transformation temperature welding materials, Weld. World 61 (4) (2017) 769–788.

[12] S. Ravi, V. Balasubramanian, S.N. Nasser, Influences of post weld heat treatment on fatigue life prediction of strength mis-matched HSLA steel welds, Int. J. Fatigue 27 (5) (May 2005) 547–553, https://doi.org/10.1016/J.IJFATIGUE.2004.09.006.

[13] J. Moravec, J. Sobotka, I. Novakova, and S. Bukovska, Assessment the Partial Welding Influences on Fatigue Life of S700MC Steel Fillet Welds, Metals (Basel) 11 (2) (2021), doi: 10.3390/met11020334.

[14] A. Ghosh, S. Das, S. Chatterjee, P. Ramachandra Rao, Effect of cooling rate on structure and properties of an ultra-low carbon HSLA-100 grade steel, Mater. Charact. 56 (1) (2006) 59–65.

[15] S.K. Dhua, S.K. Sen, Effect of direct quenching on the microstructure and mechanical properties of the lean-chemistry HSLA-100 steel plates, Mater. Sci. Eng., A 528 (21) (Aug. 2011) 6356–6365, https://doi.org/10.1016/J.MSEA.2011.04.084.

[16] I.H. Brown, The role of microsegregation in centreline cold cracking of high strength low alloy steel weldments, Scripta Materialia 54 (3) (Feb. 2006) 489–492, https://doi.org/10.1016/J.SCRIPTAMAT.2005.09.047.

[17] M.Y. Chen, M. Gouné, M. Verdier, Y. Bréchet, J.R. Yang, Interphase precipitation in vanadium-alloyed steels: Strengthening contribution and morphological variability with austenite to ferrite transformation, Acta Materialia 64 (Feb. 2014) 78–92, https://doi.org/10.1016/J.ACTAMAT.2013.11.025.

[18] P.H.G. Dornelas, F.W.C. Farias, V.H.P.M. e Oliveira, D. de Oliveira Moraes, P.Z. Júnior, J. da Cruz Payão Filho, Influence of welding interpass temperature on Charpy V-notch impact energy of coarse-grain heat-affected zone of AISI 4130 steel pipe, Int. J. Adv. Manuf. Technol. 108 (7-8) (2020) 2197–2211.

[19] Y. Shen, X. Wan, Y. Liu, G. Li, Z. Xue, K. Wu, The significant impact of Ti content on microstructure–toughness relationship in the simulated coarse-grained heated-affected zone of high-strength low-alloy steels, Ironmaking & Steelmaking 46 (6) (Jul. 2019) 584–596, https://doi.org/10.1080/03019233.2018.1533608.

[20] J. Cui, W. Zhu, Z. Chen, L. Chen, Effect of simulated cooling time on microstructure and toughness of CGHAZ in novel high-strength low-carbon construction steel, Sci. Technol. Weld. Joining 25 (2) (Feb. 2020) 169–177, https://doi.org/10.1080/13621718.2019.1661116.

[21] M. Gouda, M. Takahashi, K. Ikeuchi, Microstructures of gas metal arc weld metal of 950 MPa class steel, Sci. Technol. Weld. Joining 10 (3) (Jun. 2005) 369–377, https://doi.org/10.1179/174329305X40714.

[22] R. Dantas, et al., Evaluation of multiaxial high-cycle fatigue criteria under proportional loading for S355 steel, Eng. Failure Anal. 120, p. 105037, Feb. 2021, doi: 10.1016/J.ENGFAILANAL.2020.105037.

[23] N. Muhayat, Y.A. Matien, H. Sukanto, Y.C.N. Saputro, Triyono, Fatigue life of underwater wet welded low carbon steel SS400, Heliyon 6 (2) (2020) e03366.

[24] R. Baptista, T. Santos, J. Marques, M. Guedes, V. Infante, Fatigue behavior and microstructural characterization of a high strength steel for welded railway rails, Int. J. Fatigue 117 (Dec. 2018) 1–8, https://doi.org/10.1016/J.IJFATIGUE.2018.07.032.

[25] H.V. Ribeiro, C.A. Reis Pereira Baptista, M.S. Fernandes Lima, M.A. Santos Torres, J.B. Marcomini, Effect of laser welding heat input on fatigue crack growth and CTOD fracture toughness of HSLA steel joints, J. Mater. Res. Technol. 11 (2021) 801–810.

[26] S. Kainuma, M. Yang, Y.S. Jeong, S. Inokuchi, A. Kawabata, D. Uchida, Experimental investigation for structural parameter effects on fatigue behavior of rib-to-deck welded joints in orthotropic steel decks, Eng. Fail. Anal. 79 (Sep. 2017) 520–537, https://doi.org/10.1016/J.ENGFAILANAL.2017.04.028.

[27] D.-H. Jung, J.-K. Kwon, N.-S. Woo, Y.-J. Kim, M. Goto, S. Kim, S–N Fatigue and Fatigue Crack Propagation Behaviors of X80 Steel at Room and Low Temperatures, Metall. Mater. Trans. A 45 (2) (2014) 654–662, https://doi.org/10.1007/s11661-013-2012-4.

[28] D. Jeong, T. Park, J. Lee, S. Kim, Ambient and cryogenic S-N fatigue behavior of Fe15Mn steel and its weld, Met. Mater. Int. 21 (3) (2015) 453–460, https://doi.org/10.1007/s12540-015-4397-7.

[29] Z. Lei, Y. Hong, J. Xie, C. Sun, A. Zhao, Effects of inclusion size and location on very-high-cycle fatigue behavior for high strength steels, Mater. Sci. Eng., A 558 (Dec. 2012) 234–241, https://doi.org/10.1016/J.MSEA.2012.07.118.

[30] E. Maleki, O. Unal, K. Reza Kashyzadeh, Fatigue behavior prediction and analysis of shot peened mild carbon steels, Int. J. Fatigue 116 (2018) 48–67.

[31] R. Pamnani, T. Jayakumar, M. Vasudevan, T. Sakthivel, Investigations on the impact toughness of HSLA steel arc welded joints, J. Manuf. Processes 21 (Jan. 2016) 75–86, https://doi.org/10.1016/J.JMAPRO.2015.11.007.

[32] H.H. Wang, G.Q. Li, X.L. Wan, H.H. Wang, K.C. Nune, Y. Li, K.M. Wu, Microstructural characteristics and impact toughness in YS690MPa steel weld metal for offshore structures, Sci. Technol. Weld. Joining 22 (2) (2017) 133–142.

[33] D.M. Viano, N.U. Ahmed, G.O. Schumann, Influence of heat input and travel speed on microstructure and mechanical properties of double tandem submerged arc high strength low alloy steel weldments, Sci. Technol. Weld. Joining 5 (1) (Feb. 2000) 26–34, https://doi.org/10.1179/stw.2000.5.1.26.

[34] Z. Praunseis, T. Sundararajan, M. Toyoda, M. Ohata, The influence of soft root on fracture behaviors of high-strength, low-alloyed (HSLA) steel weldments, Mater. Manuf. Processes 16 (2) (Mar. 2001) 229–244, https://doi.org/10.1081/AMP-100104303.

[35] J.L. Caron, S.S. Babu, J.C. Lippold, Welding-induced microstructure evolution of a Cu-bearing high-strength blast-resistant steel, Metall. Mater. Trans. A 42 (13) (2011) 4015–4031, https://doi.org/10.1007/s11661-011-0801-1.

[36] P. Hariprasath, P. Sivaraj, V. Balasubramanian, S. Pilli, K. Sridhar, Effect of the welding technique on mechanical properties and metallurgical characteristics of the naval grade high strength low alloy steel joints produced by SMAW and GMAW, CIRP J. Manuf. Sci. Technol. 37 (May 2022) 584–595, https://doi.org/10.1016/J.CIRPJ.2022.03.007.

[37] K. Asim, K. Sripichai, J. Pan, Fatigue behavior of laser welds in lap-shear specimens of high strength low alloy steel sheets, Int. J. Fatigue 61 (Apr. 2014) 283–296, https://doi.org/10.1016/J.IJFATIGUE.2013.10.019.

[38] M. Shome, O.N. Mohanty, Continuous cooling transformation diagrams applicable to the heat-affected zone of HSLA-80 and HSLA-100 steels, Metall. Mater. Trans. A 37 (7) (2006) 2159–2169, https://doi.org/10.1007/BF02586136.

[39] S. Ravi, V. Balasubramanian, S.N. Nasser, Effect of notch location on fatigue crack growth behavior of strength-mismatched high-strength low-alloy steel weldments, J. Mater. Eng. Perform. 13 (6) (2004) 758–765, https://doi.org/10.1361/10599490420566.
[40] W.L. Costin, O. Lavigne, A. Kotousov, A study on the relationship between microstructure and mechanical properties of acicular ferrite and upper bainite, Mater. Sci. Eng., A 663 (Apr. 2016) 193–203, https://doi.org/10.1016/J.MSEA.2016.03.103.
[41] C. Zhang, J. Yang, X. Hu, P. Lu, M. Zhao, Microstructure characteristics and fatigue properties of welded HSLA with and without buffer layer, Mater. Sci. Eng., A 546 (Jun. 2012) 169–179, https://doi.org/10.1016/J.MSEA.2012.03.048.
[42] S. Ravi, V. Balasubramanian, S. Babu, S.N. Nasser, Assessment of some factors influencing the fatigue life of strength mis-matched HSLA steel weldments, Mater. Des. 25 (2) (Apr. 2004) 125–135, https://doi.org/10.1016/J.MATDES.2003.09.016.
[43] Y. Liu, K.S. Tsang, N.A. Subramaniam, J.H.L. Pang, Structural fatigue investigation of thermite welded rail joints considering weld-induced residual stress and stress relaxation by cyclic load, Eng. Struct. 235 (May 2021), 112033, https://doi.org/10.1016/J.ENGSTRUCT.2021.112033.
[44] D. Tchoffo Ngoula, H.T. Beier, M. Vormwald, Fatigue crack growth in cruciform welded joints: Influence of residual stresses and of the weld toe geometry, Int. J. Fatigue 101 (2017) 253–262.
[45] X.J. Yan, D.Z. Yang, M. Qi, Rotating–bending fatigue of a laser-welded superelastic NiTi alloy wire, Mater. Charact. 57 (1) (Jul. 2006) 58–63, https://doi.org/10.1016/J.MATCHAR.2005.12.009.
[46] M.J. Khameneh, M. Azadi, Evaluation of high-cycle bending fatigue and fracture behaviors in EN-GJS700-2 ductile cast iron of crankshafts, Eng. Fail. Anal. 85 (Mar. 2018) 189–200, https://doi.org/10.1016/J.ENGFAILANAL.2017.12.017.
[47] T. Lahtinen, P. Vilaça, V. Infante, Fatigue behavior of MAG welds of thermo-mechanically processed 700MC ultra high strength steel, Int. J. Fatigue 126 (Sep. 2019) 62–71, https://doi.org/10.1016/J.IJFATIGUE.2019.04.034.
[48] S. Ravi, V. Balasubramanian, S. Babu, S. Nemat Nasser, Influences of MMR, PWHT and notch location on fatigue life of HSLA steel welds, Eng. Fail. Anal. 11 (4) (2004) 619–634.
[49] H.C. Yıldırım, G. Marquis, C.M. Sonsino, Lightweight design with welded high-frequency mechanical impact (HFMI) treated high-strength steel joints from S700 under constant and variable amplitude loadings, Int. J. Fatigue 91 (Oct. 2016) 466–474, https://doi.org/10.1016/J.IJFATIGUE.2015.11.009.
[50] Y. Zhang, B. Xu, H. Wang, P. He, Z. Xing, B. Fan, An experimental analysis of fatigue behavior of a welded impeller made by FV520B stainless steel in an over-speed preloading process, Eng. Fail. Anal. 59 (Jan. 2016) 111–121, https://doi.org/10.1016/J.ENGFAILANAL.2015.09.006.
[51] A. Sarkar, A. Nagesha, Elevated temperature fatigue behaviour of structural materials for advanced ultra supercritical application, Mater. High Temp. 36 (6) (Nov. 2019) 471–478, https://doi.org/10.1080/09603409.2019.1638604.